ISTITUTO NAZIONALE DI FISICA NUCLEARE

Sezione di Roma 2

INFN/TC–98/23
11 Settembre 1998

L. Cerrito, M. Gatta, L. Paoluzi, E. Santovetti:

CLUSTER COUNTING IN A LARGE DRIFT CHAMBER IN He 80% – CH_4 20% AT NORMAL CONDITIONS

PACS: 06.70.Dn

Published by ***SIS–Pubblicazioni***
Laboratori Nazionali di Frascati

INFN – Istituto Nazionale di Fisica Nucleare
Sezione di Roma 2

INFN/TC–98/23
11 Settembre 1998

CLUSTER COUNTING IN A LARGE DRIFT CHAMBER IN He 80% – CH_4 20% AT NORMAL CONDITIONS

L. Cerrito, M. Gatta, L. Paoluzi, E. Santovetti

INFN–Sezione di Roma 2 and Physics Department of the 2nd University of Rome,
Via della Ricerca Scientifica 1, Tor Vergata, I–00133 Roma, Italy

Abstract

Results on the measurement of the primary ionization in a drift chamber operating in a mixture He 80% - CH_4 20% at normal conditions are presented. The data, collected at CERN (PS T9 beam), indicate that the cluster counting technique allows a substantial improvement with respect to the more traditional measurements. π/K separation of $\simeq 3.6\sigma$ at 4 GeV was obtained over the entire volume of the chamber: 144 (3×3) cm^2 cells with an average tracks path length of 120 cm.

1 Introduction

The energy loss of a charged particle in a medium involves discrete acts of excitation and ionization uniformly distributed along the particle path. In same cases the energy of these primary electrons is sufficiently high to produce secondary electrons. Usually these electrons are produced more closely in space than the ones due to primary ionization, so clusters of electrons are formed along the track. The electrons multiplicity of a cluster has a large variance. The most commonly used method to measure the energy loss samples the total charge in small cells and reduces the variance by discarding (30-40)% of the highest values. A measurement of the number of clusters produced in a large volume drift chamber would be a better way to identify particles, because the Poisson distribution of the number of cluster has a greater analysing power than the Landau distribution.

In 1969 Davidenko et al. [1] pointed out the advantage of measuring primary ionization with respect to the charge integration method and performed some measurements using a streamer chamber at low pressure. The main problem one faces in cluster counting (CC) is the short time between electrons at normal condition. Since then, several attempts have been made to measure primary ionization (PI) [1, 2]. In 1979-1980 Walenta built and tested a time expansion chamber to spread the clusters in time [3, 4]. With this chamber he obtained interesting results and showed that a significant part of the relativistic rise is due to the production of primary electrons. In their careful simulation of the energy loss, Lapique and Piuz [5] show that up to $\beta\gamma$ of 100 the relativistic rise is essentially due to primaries, while at higher $\beta\gamma$ the primaries production plateau is reached and the relativistic rise is mainly due to the increase in energy transfer to the secondaries. Pansky et al. [6] used a fast photomultiplier to detect photons emitted in the avalanche, to evaluate PI.

Late improvements in electronics integration, allow to use an electronic readout to measure the PI in a drift chamber at normal conditions. The cluster counting method is based on a compromise between cluster density, gas diffusion and time resolution. Helium based gas mixtures have been proposed for drift chamber in new experiments to reduce the multiple scattering contribution to momentum measurement. Helium has the additional advantage to have the clusters well separated in space, giving a sufficiently large separation in the arrival time at the sense wire to be detected individually.

2 Setup

The setup used in the test is described in details in e separated paper [9]. Briefly the chamber includes 144 (3×3) cm^2 cells arranged in 7 layers 20 cells each. A particle crossing the chamber ionises 60 cm of gas. The mixture we used was He - CH_4 (80-20)% in volumes. The preamplifiers mounted on the endplates feature 0.7 GHz Band Width, and about 200 Equivalent Noise Electrons. The chamber has been operated at a gain as low as possible ($\sim 3 \times 10^3$), to reduced observed effects of ions recombination and obviously pileup. The gas gain has been measured from the total chamber current and the known number of particles in the incoming beam spill. The signal of each cell is digitised at 1 Gsamples/sec during 2 μsec [1]. The test setup we used included a time of flight system to identify the particle species with 200 ps resolution on 25 m of flight path. Figure 1 shows the TOF histogram for a 3 GeV/c momentum beam.

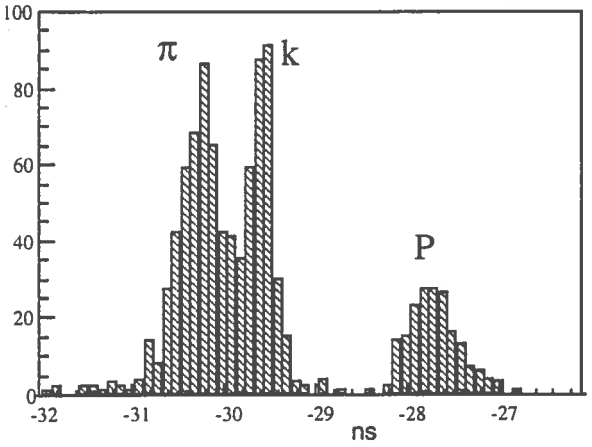

Figure 1: TOF of the 3 GeV/c momentum particles. Peaks relative to pions, kaons and protons are indicated.

[1] The digitisers, now available on the market, have been developed in a joint venture between INFN and Tektronix. Each of the 4 channels of the VXI module, Tektronix TVS 645, features 1GHz BW, up to 5 Gsample/sec at 8 bit resolution,

3 Collected data

We acquired about 7000 events per point of beam energy. Table 1 summarises all our collected data. Together with the energy, we report type of trigger, relative population and $\beta\gamma$ of pions, kaons and protons.

Table 1: Summary of data collected: for each momentum beam we reported the trigger we used to identify different particles, the relative population (R) of the particle inside the beam and its $\beta\gamma$. For the trigger, T are track defining scintillators while S1 is the TOF set of counters and TC1 a Cherenkov counter to reduce the number of high β particles.

momentum	trigger	π		K		P	
GeV/c		R(%)	$\beta\gamma$	R(%)	$\beta\gamma$	R(%)	$\beta\gamma$
1^+	T*S1*TC1	74	7.14			21	1.06
1.5^+	T*S1*TC1	78	10.7			18	1.60
2^+	T*S1*TC1	74	14.3			22	2.13
3^-	T*S1*TC1	46	21.4	34	6.12	20	3.19
4^+	T*S1	65	28.6	5	8.16	23	4.25
4^-	T*S1*TC1	31	28.6	32	8.16	26	4.25
5^-	T*S1*TC1					10	5.32
5^+	T*S1*TC1					100	5.32
15^-	T*S1	100	107				16.0

4 Data analysis

In reference [9] the performances of the chamber are described in details. Figure 2 shows on the spatial resolution obtained with our setup.

In particular, using the digitised signal data, a fit of the leading edge of the first electron can be used to free the t_0 measurement from the time jitter induced by amplitude fluctuation. Figure 3 shows a typical waveform signal reconstructed offline.

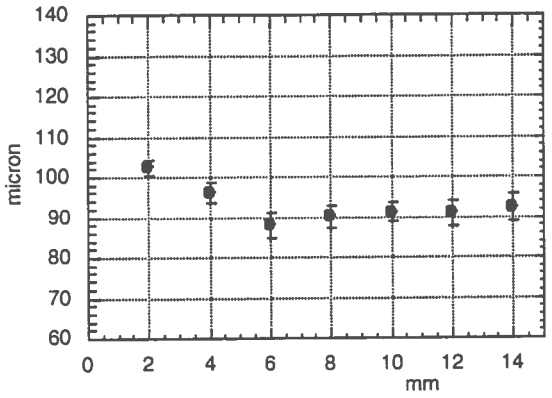

Figure 2: Spatial resolution versus impact parameter.

32 kbytes RAM. The "autoadvance" mechanism allowed us to collect up to 10 events per spill before to open the readout channel in the inter-spill time

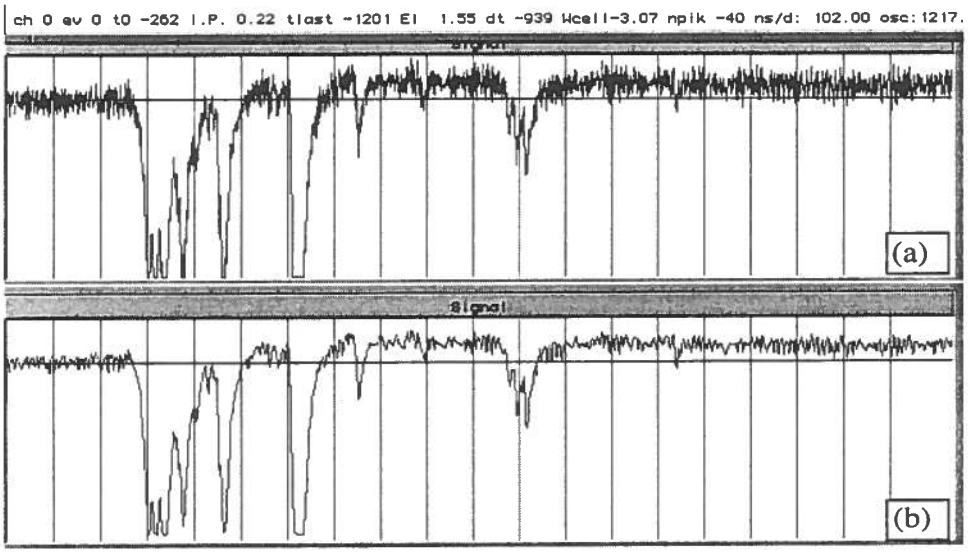

Figure 3: The first signal of the run 104 (4 GeV/c momentum) is shown. In a) we plot the raw data signal while in b) the signal after the 500 MHz software lowpass filer. The full 2 μs of signal is displayed and each division corresponds to 100 ns.

The vertical range is 50 mV (from +10 mV to -40 mV) and the horizontal one is 2 μsec with 100 ns per div. The signal is amplified by a factor of 100. Being the chamber gain set at about 3×10^3 and having the cell an impedance of 470 Ohms, we expect for a single electron signal about 4.8 mV, i.e. about 10% of the vertical range, if we further assume an average width for smaller signal of about 5 ns. The rms of the noise is about 1 mV. The single electron signal detection is difficult but feasible and special care has to be devoted to the analysis in order to obtain an high efficiency in peaks recognition. Several algorithms have been tested and in particular an integration followed by a derivative process. We soon noticed that any algorithm based purely on the frequency cannot be used because, as the noise, the true signal has a flat spectrum due to the ensemble of different effects like fluctuations in amplification, spread in the arrival time, overlap of different signals etc. Something more complex is needed. Our algorithm is based on the charge released in the peak when calculated over the correct baseline. Anyway, before the peaks finding, unnecessary high frequencies are discarded.

4.1 Frequency filter

A dedicated MonteCarlo code was developed for electron transport and gas multiplication, keeping into account, beside traditional effects, the field due to positive ions. Our simulation predicts a rise time of the signal pulse of 2.5 ns. The MonteCarlo prediction was then checked experimentally using an extra fast electronics on a drift tube. We found a good agreement with our simulation. Data collected were analysed keeping in mind that, as noted before, both simulation and experiment showed an upper cut off frequency of 500 MHz. In figure 3 is shown the raw data signal (a) and the same signal after software filtering has been applied to the data (b).

4.2 Base line

The correct value of the charge contained in a peak is obtained integrating the peak area over an opportune base line, calculated from the previous part of the signal. Its calculation takes into account the residual charge in the cell after electrons collection, the positive ions moving slowly toward the cathode plus the discharge time of the overall capacitance over the 470 Ohms impedance. A parametrisation of the image charge of the ions moving 1000 times slower than electrons plus the constant time of the capacitance allowed us to calculate the base line seen by further electrons approaching the sense wire. In figure 4, together with the signal, is shown the calculated base line. As one should expect, this base line goes to the average value of the noise when the signal goes off.

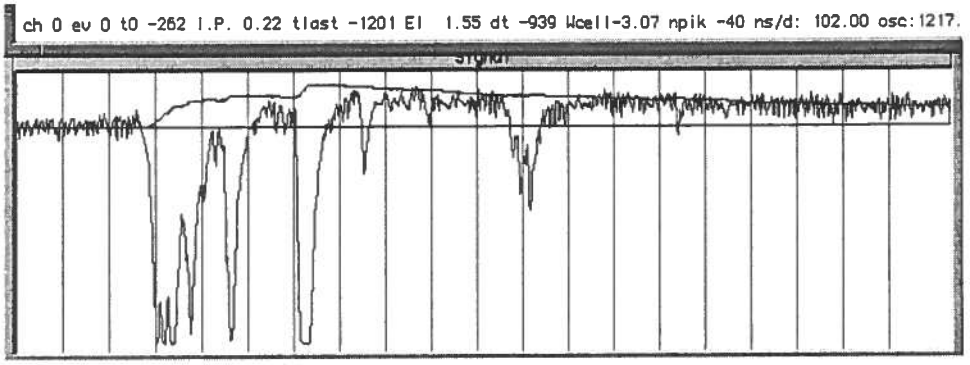

Figure 4: The same signal as before is shown. The line surrounding the waveform shows the base line calculated by the charge released in the cell. Ending the signal the charge line goes to become the average value of the noise swing.

4.3 Peak counting

Three different patterns are considered peaks. First a "fall" followed by a "rise"; second a "fall" followed by a "flat"; third a "rise" followed by a "flat". We define a "flat" as a double change of concavity of the signal, during its fall or its rise. In the last two cases the peak is assigned to the end of the flat part. As mentioned before, the peak charge is evaluated respect to the correct baseline produced by all the previous peaks. In the 150 ns preceding the trigger, where there are no peaks, the mean value of the peak area is calculated. Then each peak, from 0 to 2 μs, whose the charge exceeds 2 times the overage noise value is tagged as a signal. The number 2 has been set as the lowest value which allows do not count peaks before the trigger. In figure 5 we show the histogram of the number of counted peaks per cell for pions of 3 GeV/c momentum.

The figure shows the typical Landau shape, indicating that, beside primaries, we are counting secondaries too.

As mentioned above, the CC relays on the assumption that the average distance between secondaries is smaller than the distance between clusters. To discard secondaries we blind the analysis after a peak is detected for a time window longer than the cluster size, but shorter than the distance between different clusters (blindness cut). The cluster size is related to the diffusion of the electrons in the gas and depend on the gas type and their drift time. In figure 6 the average distance between primaries vs the track impact parameter is reported together with the longitudinal diffusion as reported in ref. [10].

The analysis with different blindness cut values over all the possible track impact parameters shows that a value of 15 ns maximizes the ratio of the primaries detection efficiency over secondaries rejection. Figure 7 shows the signal with a vertical bars indicating the tagged peaks after application of the blindness cut.

Figure 8 shows the new histogram of figure 5. The Landau fit of the histogram of figure 5 gives a mean value of 28.5 peaks while the gaussian fit of figure 8 gives a mean value of 19.7. From this we have $< N_{no-Bcut} > / < N_{Bcut} >= 1.45$. The values we find is lower than the number of secondaries

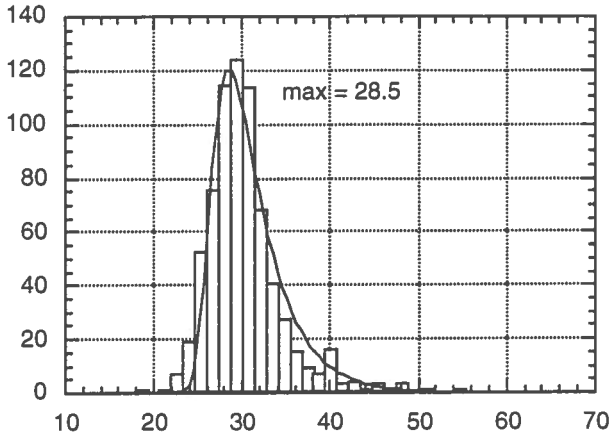

Figure 5: The figure shows the histogram of the counted peaks per cell for pions of 3 GeV/c momentum. The fit with a Landau function features a most probable value of 28.5.

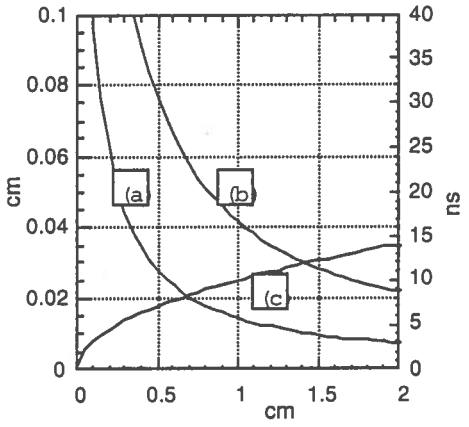

Figure 6: Average distance in the electron arrival time versus impact parameter with full counting efficiency (a) and with 90% counting efficiency (b). In (c) the longitudinal diffusion is shown.

per primary, 1.6, reported in ref [11]. This is due to a still present contamination of secondaries in our final sample, as is also visible from the shape of the histogram of figure 8.

4.4 χ^2

Using the track reconstruction, we selected clean tracks on the basis of tracking χ^2. Furthermore we required at least 10 hit cells over 20 on the track. The average number of hit cells on good tracks is 14.

4.5 Tracks summing

As far as cluster counting is concerned signal in different cells can be considered as independent events and summed together. In order to have a larger cells statistic we combined three tracks tagged from the TOF as same particle. The resulting track length we obtained is shown in figure 9, in terms of number of cells.

5 Results

Of the 7000 events we collected at each beam momentum 82% have been used for resolution measurement. Results are summarised in table 2.

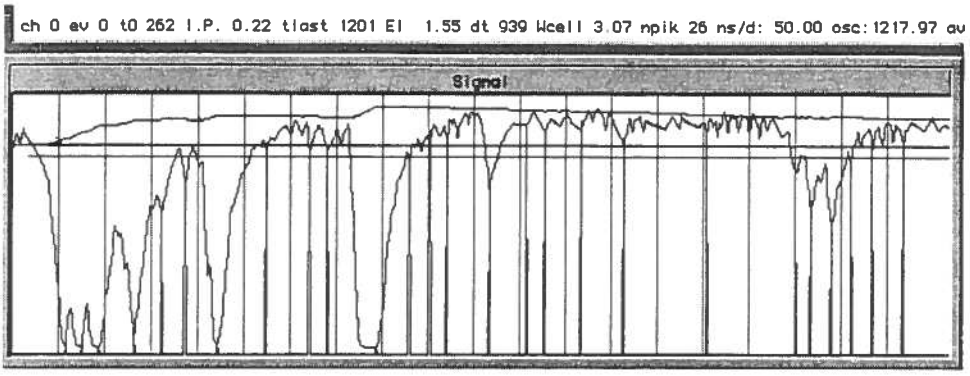

Figure 7: Always for the same signal, zoomed between 250 ns and 1250 ns after the trigger, the vertical lines show those peaks where we found a charge larger than the threshold and after the blindness cut application (see text).

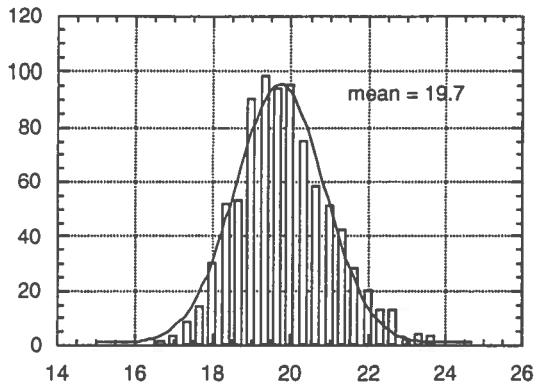

Figure 8: Same data of figure 5 after applying the blindness cut at 15 ns. The fit with the gaussian function gives an central value of 19.7.

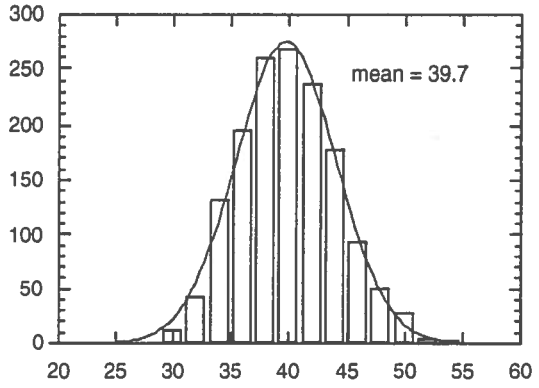

Figure 9: Cell multiplicity for 3 GeV/c momentum pions. The histogram is the resulting after the χ^2 cut and three events track summing. The central value of the gaussian fit is 39.7.

As a check of our data, we developed a calculation of primary ionization [8], based on the Allison and Cobb approach (PAI model) [7]. The model calculations are compared with the data in figure 10, taking also into account our cluster counting efficiency.

We don't have at the moment a firm estimate of our systematics. Two main effects have been identified: stability of the beam momentum value and the gas flow controllers jitter. We estimate an upper limit to this effects to be (5-10)%.

In figure 11 we plot the dN/dx resolution we get from the samples of pions, kaons and protons.

The resolution improves for higher values of $\beta\gamma$, as one would expect from the relativistic rise of the number of clusters. Together with the dN/dx resolution, we report also the resolution obtained wit traditional methods (see above) with a truncated mean at 70%. Our analysis refers to events with average (3×3) cm^2 cell multiplicity of 40 (see fig. 9). The resolution values are marginally worse than the poissonian expected ones, most probably because of some contamination of secondaries in our data samples. Figure 12 shows the poissonian index δ, defined as $\delta = \sigma/\sqrt{n}$, for pions, kaons and protons versus their $\beta\gamma$. For a pure poissonian distribution we would expect to find $\delta = 1$.

An other result quoted for Helium is by G. Finocchiaro et al. [12]. They report a measurement of energy loss for 50 GeV/c momentum pions with a resolution of 3% using 100 samples and a truncated mean at 80%. If we extrapolate our 3.4% resolution for pions at 15 GeV/c from 40 to 100 cells we obtain a dN/dx resolution for this particles of 2.15%. As a further figure of merit of the Cluster Counting method we can compare our dN/dx resolution to the dE/dx resolution obtained, at normal condition, in gas mixture based on Argon which is 20 times heavier than the Helium. The best one we found in literature

6 Conclusions

The data presented show that it is possible to use the Cluster Counting method in a large volume drift chamber at normal pressure. Helium based mixtures are particularly suited for this purpose. The large data volumes and cost per channel can be overcome with an appropriate electronics. Beside the main goal of particle identification, the system can be used to perform an absolute measurement of the ionization in different gases.

References

[1] A. Davidenko et al.;
Nuclear Instruments and Methods **67**, 325 (1969)

[2] V. Eckardt et al.;
Nuclear Instruments and Methods **143**, 235 (1977)

[3] A. H. Walenta;
IEEE Transaction on Nuclear Science, **NS-26**, No.1 (1979)

[4] P. Rehak and A. H. Walenta;
IEEE Transaction on Nuclear Science, **NS-27**, No.1 (1980)

[5] F. Lapique and F. Piuz;
Nuclear Insruments and Methods **175**, 297 (1980)

[6] A. Pansky et al.;
Nuclear Instruments and Methods **67**, 325 (1969)

[7] W. W. M. Allison and J. H. Cobb;
Ann. Rev. Part. Sci. **30**, 253 (1980)

[8] E. Santovetti et al.;
INFN/TC **97/3**, (1997)

[9] L. Cerrito et al.;
INFN/TC **96/20**, (1996)

[10] J. Va'vra et al.;
La Biodola Conference 1991, may 25 (1969)

[11] S. M. Playfer et al.;
ETHZ-IMP **91** (1991)

[12] G. Finocchiaro et al.;
....., (1995)

[13] M. Hauscild et al.;
Nuclear Instruments and Methods **A 379**, 436 (1996)

[14] F. Sauli;
CERN Report **77-09** (1977)